Excitation spectrum of Fe^{2+} in a tetrahedral potential: Dynamic Jahn-Teller effect

David Colignon and E. Kartheuser
Institut de Physique, Université de Liège, Sart-Tilman, B-4000 Liège 1, Belgium

Sergio Rodriguez
Department of Physics, Purdue University, West Lafayette, Indiana 47907-1396

Murielle Villeret
Department of Mathematics, City University, London EC1V 0HB, United Kingdom
(Received 11 October 1994)

A theoretical study is given of the vibronic energy levels of doubly ionized iron in the tetrahedral potential of a II-VI compound. The orbital doublet and triplet states of Fe^{2+} experience energy shifts due to the spin-orbit and spin-spin interactions and to Jahn-Teller couplings of the doublet and triplet manifolds with overtones of phonons of Γ_3 and Γ_5 symmetries, respectively. The positions of the optical absorption lines in the near and far infrared are accounted for with excellent accuracy taking the orbital splitting $\Delta=2530\ \mathrm{cm}^{-1}$, spin-orbit coupling $\lambda=-95\ \mathrm{cm}^{-1}$, spin-spin interaction $\rho=0.7\ \mathrm{cm}^{-1}$, and Jahn-Teller interactions $E_{\mathrm{JT}}^{(3)}=2\ \mathrm{cm}^{-1}$ and $E_{\mathrm{JT}}^{(5)}=275\ \mathrm{cm}^{-1}$ describing coupling between the $3d$ electrons and phonons of energies $\hbar\omega_3=28\ \mathrm{cm}^{-1}$ and $\hbar\omega_5=40\ \mathrm{cm}^{-1}$ of symmetries Γ_3 and Γ_5, respectively. The oscillator strengths (electric- and magnetic-dipole) are obtained for transitions within states in the orbital doublet as well as between these levels and the orbital triplet.

I. INTRODUCTION

The present paper deals with an investigation of the energy-level spectrum of doubly ionized iron in a tetrahedral environment. A first approach to this study is based on the crystal-field theory. The ^5D term of the free ion separates into an orbital doublet and an orbital triplet, where the former lies below the latter in energy. The energy of separation is denoted here by Δ. Following the nomenclature of Koster *et al.*,[1] we denote these manifolds by $^5\Gamma_3$ and $^5\Gamma_5$, respectively. The spin-orbit interaction splits the tenfold $^5\Gamma_3$ level into five, approximately equidistant, levels of symmetries Γ_1, Γ_4, Γ_3, Γ_5, and Γ_2, listed in order of increasing energy. The orbital angular momentum $\mathbf{L}$ of these levels is quenched so that, in first order in the spin-orbit interaction, $\lambda\mathbf{L}\cdot\mathbf{S}$, the separations of these states vanish. Here $\mathbf{S}$ is the total spin operator of the ion, and λ the strength of the spin-orbit coupling. In second order in λ, admixture of the $^5\Gamma_3$ and $^5\Gamma_5$ multiplets leads to the above-mentioned splittings in which adjacent levels are separated by $6\lambda^2/\Delta$. The fifteenfold degenerate $^5\Gamma_5$ manifold splits in first order in λ as if it had an effective orbital angular momentum $\mathbf{I}$ with $I=1$ and a spin-orbit coupling equal to $-\lambda\mathbf{I}\cdot\mathbf{S}$. Defining $\mathbf{F}=\mathbf{I}+\mathbf{S}$, since $S=2$, the $^5\Gamma_5$ states split into levels whose additional energies are 3λ, λ, and -2λ and degeneracies 3, 5, and 7 corresponding to $F=1$, 2, and 3, respectively. In second order these degeneracies are lifted further. For $F=1$, the symmetry is characterized by Γ_5 which, for iron ($\lambda<0$), is the lowest electronic level originating from the $^5\Gamma_5$ multiplet. For $F=2$, the level splits into a triplet Γ_4 and a double Γ_3, while for $F=3$ the splitting is described by $\Gamma_5+\Gamma_4+\Gamma_1$. The electron-phonon interaction couples these states with the vibrational modes of the crystal and their overtones, giving rise to a series of energy levels. These are described as vibronic levels, i.e., admixtures of electronic and vibrational excitations.

Optical-absorption due to the presence of transition-metal ions of the iron group in compound semiconductors has been investigated by many authors.[2–7] Slack, Ham, and Chrenko[2] studied the near-infrared spectrum of Fe^{2+} in ZnS, CdTe, and $MgAl_2O_4$, while Baranowski, Allen, and Pearson[3] investigated the same spectral region in a number of II-VI and III-V compounds with iron and cobalt. More recently Udo *et al.*[6] investigated the transmission of CdTe:Fe^{2+} and CdSe:Fe^{2+} in the near infrared. Far-infrared absorption measurements of the excitation spectrum of Fe^{2+} in ZnS were carried out by Slack, Roberts, and Ham[4] and in CdTe by Slack, Roberts, and Vallin,[5] who also extended their measurements to the far infrared. Testelin *et al.*[7] investigated the far-infrared absorption of CdTe:Fe^{2+}.

Crystal-field theory accounts for the general form of the excitation spectrum but fails to provide an explanation for the spacing of the energy levels in the $^5\Gamma_3$ and $^5\Gamma_5$ multiplets or for additional transition which do not find a place in this theoretical model.[4,6] To account for these discrepancies, Slack, Ham, and Chrenko[2] proposed a model in which the $^5\Gamma_5$ multiplet is modified by a strong coupling of the $3d$ electrons of the magnetic ion with vibrational modes of the host crystal, i.e., the dynamic Jahn-Teller effect.[8,9]

For the purpose of this investigation, the vibrational modes of the crystal are best classified according to the site symmetry of the magnetic ion rather than according to the space group of the host. From symmetry con-

siderations, it follows that matrix elements of the electron-phonon interaction, H_{ep}, between states in the ${}^5\Gamma_3$ multiplet vanish for a phonon mode of symmetry Γ_5, while matrix elements between states in the ${}^5\Gamma_5$ multiplet need not vanish for phonons of symmetries Γ_3 and Γ_5.

The dynamic Jahn-Teller effect on the ${}^5\Gamma_3$ multiplet of Fe^{2+} coupled to a Γ_3 phonon was investigated by Vallin[10] and, later, by Testelin *et al.*[7] Vallin concluded that the far-infrared excitation spectrum of Fe^{2+} in CdTe is consistent with a weak Jahn-Teller energy of $E_{JT}=4.2$ cm^{-1}, assuming a phonon energy $\hbar\omega=38$ cm^{-1}. Testelin *et al.*[7] reach similar conclusions but fit their data with $E_{JT}=2.5\pm0.3$ cm^{-1} and $\hbar\omega=28\pm0.5$ cm^{-1}. Rivera-Iratchet, de Orúe, and Vogel[11] considered the near-infrared data of Refs. 2 and 5 for Fe^{2+} in CdTe using $E_{JT}=240$ cm^{-1} and a Γ_3 phonon of energy $\hbar\omega=40$ cm^{-1}. Martinelli, Passaro, and Pastori Parravicini[12] have made an analysis of the near-infrared absorption in CdTe:Fe^{2+} using Haydock's recursive method.[13] They fit the data with $E_{JT}=232$ cm^{-1} and a Γ_3 phonon of energy $\hbar\omega=36$ cm^{-1} ($\Delta=2585$ cm^{-1} and $\lambda=-100$ cm^{-1}). Savona, Bassani, and Rodriguez[14] have made a study of the oscillator strengths and of the dynamic Jahn-Teller effect in CdTe:Fe^{2+}. On the basis of the evidence involving phonon-assisted transitions,[6] they argued that the energy levels in the ${}^5\Gamma_5$ multiplet of Fe^{2+} are modified by a strong coupling to a Γ_5 phonon. Agreement with the data[2,6] is obtained with a Jahn-Teller stabilization energy $E_{JT}=255$ cm^{-1} and a phonon energy $\hbar\omega\approx40$ cm^{-1}, in substantial accord with Ref. 2.

In this paper we describe both the near- and far-infrared spectra of Fe^{2+} in CdTe consistently using the same material parameters. Specifically, we consider a strong electron-phonon coupling between the electronic states of the ${}^5\Gamma_5$ multiplet with a phonon of symmetry Γ_5 and a weaker one between the ${}^5\Gamma_3$ states and a Γ_3 phonon.

The analysis of this work is described in Secs. II–IV. Section II displays the effective Hamiltonian of the Fe^{2+} ion in the tetrahedral potential together with the electron-phonon coupling, while Sec. III is concerned with the calculation of the energy levels. Section IV is devoted to the study of the selection rules and oscillator strengths for optical transitions. Comparison with experimental work and further discussion form the subject of Sec. V. For convenience here we give the numerical values of the parameters appropriate for an isolated Fe^{2+} at a cation site in CdTe, as obtained in this work. With the notation used here we have $\Delta=2530$ cm^{-1}, $\lambda=-95$ cm^{-1}, and the spin-spin interaction parameter $\rho=0.7$ cm^{-1}. The Γ_5 phonon, of energy $\hbar\omega=40$ cm^{-1}, interacts with the ${}^5\Gamma_5$ multiplet of Fe^{2+} with a Jahn-Teller stabilization energy $E_{JT}=275$ cm^{-1}. The electron-phonon coupling used for the ${}^5\Gamma_3$ multiplet is characterized by $E_{JT}=2$ cm^{-1} and $\hbar\omega=28$ cm^{-1}, the symmetry of the phonon being Γ_3.

II. EFFECTIVE HAMILTONIAN

The ${}^5D$ term of the free Fe^{2+} ion in a field of T_d symmetry splits into an orbital doublet (Γ_3) and an orbital triplet (Γ_5), as we already mentioned in Sec. I. Denoting by $|M_L\rangle$ ($M_L=2$, 1, 0, -1, and -2) the orbital wave functions of the free ion, the symmetry-adapted state vectors in the crystal field are

$$\Gamma_3:\begin{cases}\gamma_1=|0\rangle\\ \gamma_2=2^{-1/2}(|2\rangle+|-2\rangle)\end{cases} \tag{1}$$

and

$$\Gamma_5:\begin{cases}\epsilon_1=i2^{-1/2}(|1\rangle+|-1\rangle)\\ \epsilon_2=2^{-1/2}(-|1\rangle+|-1\rangle)\\ \epsilon_3=i2^{-1/2}(-|2\rangle+|-2\rangle).\end{cases} \tag{2}$$

The state vectors γ_1 and γ_2 behave as $2z^2-x^2-y^2$ and $\sqrt{3}(x^2-y^2)$, respectively, under the operations of T_d, and ϵ_1, ϵ_2, and ϵ_3 transform as yz, zx, and xy (or x, y, and z). The cubic axes are here called x, y, and z. The spin-wave functions are denoted by $\tilde{\gamma}_1$, $\tilde{\gamma}_2$, $\tilde{\epsilon}_1$, $\tilde{\epsilon}_2$, and $\tilde{\epsilon}_3$, and their behavior under the symmetry operations is identical to that of the states listed in Eqs. (1) and (2). The ${}^5\Gamma_3$ multiplet contains the states generated by the product wave functions involving orbital and spin parts according to $\Gamma_3\otimes\tilde{\Gamma}_3=\Gamma_1\oplus\Gamma_2\oplus\Gamma_3$ and $\Gamma_3\otimes\tilde{\Gamma}_5=\Gamma_4\oplus\Gamma_5$ and are denoted by the symbols α, β, γ, δ, or ϵ depending on whether they belong to Γ_1, Γ_2, Γ_3, Γ_4 or Γ_5, respectively. They are displayed in Table I. In a similar fashion we obtain the states of the ${}^5\Gamma_5$ multiplet from $\Gamma_5\otimes(\tilde{\Gamma}_3\oplus\tilde{\Gamma}_5)=\Gamma_1+\Gamma_3+2\Gamma_4+2\Gamma_5$. The spin-orbit interaction is diagonalized to first order in λ by the vectors shown in Table II, i.e., the off-diagonal terms in $\mathbf{L}\cdot\mathbf{S}$ between states of the same symmetry in the ${}^5\Gamma_5$ multiplet vanish. The matrices of $\mathbf{L}\cdot\mathbf{S}$ for the different states in Tables I and II are given in the Appendix.

The effective Hamiltonian is

$$H=H_0+V_c(T_d)+\lambda\mathbf{L}\cdot\mathbf{S}+H_{SS}+H_{JT}\ , \tag{3}$$

where H_0 is the Hamiltonian of the free ion omitting the spin-orbit interaction and the spin-spin interaction[15]

$$H_{SS}=-\rho[(\mathbf{L}\cdot\mathbf{S})^2+\tfrac{1}{2}\mathbf{L}\cdot\mathbf{S}-\tfrac{1}{3}L(L+1)S(S+1)]\ . \tag{4}$$

The tetrahedral potential $V_c(T_d)$ gives the separation Δ between the ${}^5\Gamma_3$ and ${}^5\Gamma_5$ multiplets. The electron-phonon coupling H_{JT} is given by

$$H_{JT}=\hbar\omega_3\sum_{i=1}^{2}(a_i^\dagger a_i+\tfrac{1}{2})+\sum_{i=1}^{2}(a_i^\dagger+a_i)U_i^{(3)}+\hbar\omega_5\sum_{j=1}^{3}(b_j^\dagger b_j+\tfrac{1}{2})+\sum_{j=1}^{3}(b_j^\dagger+b_j)U_j^{(5)}\ . \tag{5}$$

Here a_i ($a_i^\dagger$) is a destruction (creation) operator for a phonon belonging to the i row of Γ_3. A similar statement is applicable to b_j, where j labels the rows of Γ_5; and $\hbar\omega_3$ and $\hbar\omega_5$ are the energies of phonons of symmetries Γ_3 and Γ_5, respectively. The 5×5 matrices $U_i^{(3)}$ and $U_j^{(5)}$ consist of 2×2 and 3×3 blocks along the diagonal corresponding to the matrix elements of the electron-phonon coupling between the orbital states γ_1 and γ_2 for the first block and ϵ_1, ϵ_2, and ϵ_3 for the second. The 2×2 blocks

TABLE I. Electronic wave functions for the $^5\Gamma_3$ multiplet of Fe^{2+} in a tetrahedral potential. The wave functions listed in the first column are linear combinations of the product states in the first row with the coefficients given below.

	$\gamma_1\bar{\gamma}_1$	$\gamma_1\bar{\gamma}_2$	$\gamma_2\bar{\gamma}_1$	$\gamma_2\bar{\gamma}_2$	$\gamma_1\bar{\epsilon}_1$	$\gamma_1\bar{\epsilon}_2$	$\gamma_1\bar{\epsilon}_3$	$\gamma_2\bar{\epsilon}_1$	$\gamma_2\bar{\epsilon}_2$	$\gamma_2\bar{\epsilon}_3$
$\lvert\alpha\rangle$	$\frac{1}{\sqrt{2}}$			$\frac{1}{\sqrt{2}}$						
$\lvert\beta\rangle$		$\frac{1}{\sqrt{2}}$	$-\frac{1}{\sqrt{2}}$							
$\lvert\gamma_1\rangle$	$-\frac{1}{\sqrt{2}}$			$\frac{1}{\sqrt{2}}$						
$\lvert\gamma_2\rangle$		$\frac{1}{\sqrt{2}}$	$\frac{1}{\sqrt{2}}$							
$\lvert\delta_1\rangle$					$-\frac{1}{2}\sqrt{3}$			$-\frac{1}{2}$		
$\lvert\delta_2\rangle$						$\frac{1}{2}\sqrt{3}$			$-\frac{1}{2}$	
$\lvert\delta_3\rangle$										1
$\lvert\epsilon_1\rangle$					$-\frac{1}{2}$			$\frac{1}{2}\sqrt{3}$		
$\lvert\epsilon_2\rangle$						$-\frac{1}{2}$			$-\frac{1}{2}\sqrt{3}$	
$\lvert\epsilon_3\rangle$							1			

of $U_1^{(3)}$ and $U_2^{(3)}$ are $-(\hbar\omega_3 E_{\rm JT}^{(3)})^{1/2}\sigma_z$ and $(\hbar\omega_3 E_{\rm JT}^{(3)})^{1/2}\sigma_x$ with σ_x and σ_z equal to the usual Pauli matrices. The 3×3 blocks are $-(\hbar\omega_3 E_{\rm JT}^{\prime(3)})^{1/2}(2M_3^2-M_1^2-M_2^2)$ and $-(\hbar\omega_3 E_{JT}^{\prime(3)})^{1/2}3^{1/2}(M_1^2-M_2^2)$ where M_1, M_2, and M_3 are given in Eqs. (19) in Savona, Bassani, and Rodriguez.[14] The off-diagonal blocks of $U_1^{(3)}$ and $U_2^{(3)}$ are equal to zero. The 2×2 blocks of $U_1^{(5)}$, $U_2^{(5)}$, and $U_3^{(5)}$ consist of zeros , while the 3×3 blocks are simply $(3\hbar\omega_5 E_{\rm JT}^{(5)}/2)^{1/2}M_j$ ($j=1$, 2, and 3). The off-diagonal 2×3 blocks contain the following nonvanishing matrix elements:

$$\langle\gamma_1|U_1^{(5)}|\epsilon_1\rangle=\langle\gamma_1|U_2^{(5)}|\epsilon_2\rangle=-3^{-1/2}\langle\gamma_2|U_1^{(5)}|\epsilon_1\rangle$$
$$=3^{-1/2}\langle\gamma_2|U_2^{(5)}|\epsilon_2\rangle=-\tfrac{1}{2}\langle\gamma_1|U_3^{(5)}|\epsilon_3\rangle$$
$$=-\tfrac{1}{2}\langle\hbar\omega_5 E_{\rm JT}^{\prime(5)})^{1/2}.$$

Even though symmetry considerations do not rule out

TABLE II. Electronic wave functions for the $^5\Gamma_5$ multiplet of Fe^{2+} in a tetrahedral potential. The wave functions listed in the first column are linear combinations of the product states in the first row with the coefficients given below.

	$\epsilon_1\bar{\gamma}_1$	$\epsilon_1\bar{\gamma}_2$	$\epsilon_1\bar{\epsilon}_1$	$\epsilon_1\bar{\epsilon}_2$	$\epsilon_1\bar{\epsilon}_3$	$\epsilon_2\bar{\gamma}_1$	$\epsilon_2\bar{\gamma}_2$	$\epsilon_2\bar{\epsilon}_1$	$\epsilon_2\bar{\epsilon}_2$	$\epsilon_2\bar{\epsilon}_3$	$\epsilon_3\bar{\gamma}_1$	$\epsilon_3\bar{\gamma}_2$	$\epsilon_3\bar{\epsilon}_1$	$\epsilon_3\bar{\epsilon}_2$	$\epsilon_3\bar{\epsilon}_3$
$\lvert\alpha'\rangle$			$\frac{1}{\sqrt{3}}$						$\frac{1}{\sqrt{3}}$						$\frac{1}{\sqrt{3}}$
$\lvert\gamma_1'\rangle$			$-\frac{1}{\sqrt{6}}$						$-\frac{1}{\sqrt{6}}$						$\sqrt{\frac{2}{3}}$
$\lvert\gamma_2'\rangle$			$\frac{1}{\sqrt{2}}$						$-\frac{1}{\sqrt{2}}$						
$\lvert\delta_1'\rangle$	$-\frac{1}{\sqrt{2}}$	$-\frac{1}{\sqrt{6}}$								$-\frac{1}{\sqrt{6}}$				$\frac{1}{\sqrt{6}}$	
$\lvert\delta_2'\rangle$				$\frac{1}{\sqrt{6}}$	$\frac{1}{\sqrt{2}}$	$-\frac{1}{\sqrt{6}}$							$-\frac{1}{\sqrt{6}}$		
$\lvert\delta_3'\rangle$				$-\frac{1}{\sqrt{6}}$				$\frac{1}{\sqrt{6}}$				$\sqrt{\frac{2}{3}}$			
$\lvert\delta_1''\rangle$	$\frac{1}{2}$	$\frac{1}{2\sqrt{3}}$								$-\frac{1}{\sqrt{3}}$				$\frac{1}{\sqrt{3}}$	
$\lvert\delta_2''\rangle$				$\frac{1}{\sqrt{3}}$	$-\frac{1}{2}$	$\frac{1}{2\sqrt{3}}$							$-\frac{1}{\sqrt{3}}$		
$\lvert\delta_3''\rangle$				$-\frac{1}{\sqrt{3}}$				$\frac{1}{\sqrt{3}}$				$-\frac{1}{\sqrt{3}}$			
$\lvert\epsilon_1'\rangle$	$-\frac{1}{\sqrt{10}}$	$\sqrt{\frac{3}{10}}$								$\sqrt{\frac{3}{10}}$				$\sqrt{\frac{3}{10}}$	
$\lvert\epsilon_2'\rangle$				$\sqrt{\frac{3}{10}}$	$-\frac{1}{\sqrt{10}}$	$-\sqrt{\frac{3}{10}}$							$\sqrt{\frac{3}{10}}$		
$\lvert\epsilon_3'\rangle$				$\sqrt{\frac{3}{10}}$				$\sqrt{\frac{3}{10}}$			$\sqrt{\frac{2}{5}}$				
$\lvert\epsilon_1''\rangle$	$\sqrt{\frac{3}{20}}$	$-\frac{3}{\sqrt{20}}$								$\frac{1}{\sqrt{5}}$				$\frac{1}{\sqrt{5}}$	
$\lvert\epsilon_2''\rangle$				$\frac{1}{\sqrt{5}}$	$\sqrt{\frac{3}{20}}$	$\frac{3}{\sqrt{20}}$							$\frac{1}{\sqrt{5}}$		
$\lvert\epsilon_3''\rangle$				$\frac{1}{\sqrt{5}}$				$\frac{1}{\sqrt{5}}$			$-\sqrt{\frac{3}{5}}$				

the presence of the matrix elements containing $E'^{(3)}_{JT}$ and $E'^{(5)}_{JT}$, the energy shifts are not sensitive to the values chosen for them. In fact, the quantity $E'^{(5)}_{JT}$ appears in second-order perturbation connecting Γ_3 and Γ_5 orbital states which are separated by $\Delta \sim 2500\ \mathrm{cm}^{-1}$. Thus the effect of $E'^{(5)}_{JT}$ is reduced by $E'^{(5)}_{JT}/\Delta$ which, if $E'^{(5)}_{JT}$ were of the order of $E^{(5)}_{JT}$ would be about 10^{-1}. If, as is reasonable to assume, the primed and unprimed Jahn-Teller energies are comparable, and since $E^{(3)}_{JT}$ is weak (as deduced from the comparison between the theory and the far-infrared measurements), the effect of $E'^{(3)}_{JT}$ on the ${}^5\Gamma_5$ multiplet is negligible in comparison with the effect of $E^{(5)}_{JT}$. Because of these considerations we have set $E'^{(3)}_{JT}$ and $E'^{(5)}_{JT}$ equal to zero. The results of numerical calculations in which we set $E'^{(3)}_{JT}=E^{(3)}_{JT}$ and $E'^{(5)}_{JT}=E^{(5)}_{JT}$ do not differ significantly from those in which the primed quantities are set equal to zero.

III. ENERGY LEVELS

To find the eigenvalues of the Hamiltonian operator (3) we start with a set of symmetry-adapted wave functions which are linear combinations of products of electronic and vibrational states. The phonon states and their overtones are classified according to the irreducible representations of the group T_d. We denote by $A^{(3)}(n)$, $B^{(3)}(n)$, and $C^{(3)}_i(n)$ ($i=1$ and 2), the overtones of the Γ_3 phonon; n is the order of the overtone which is taken to be $n \leq 6$. The symbols A, B, and C indicate the irreducible representation to which each overtone belongs; A, B, and C correspond to the Γ_1, Γ_2, and Γ_3 irreducible representations of T_d. Similarly we use the notations $A^{(5)}(n)$, $B^{(5)}(n)$, $C^{(5)}_i(n)$, $D^{(5)}_j(n)$, or $E^{(5)}_j(n)$ ($i=1,2$; $j=1,2,3$) to designate overtones of order n of a Γ_5 phonon which belong to the Γ_1, Γ_2, Γ_3, Γ_4 or Γ_5 irreducible representation of T_d. These states are obtained using a projection operator formalism. Care must be taken, when for given n there are two or more overtones of the same symmetry, to ensure that the states are chosen to be orthogonal to one another. In Table III we give the classification of the overtones of a Γ_3 phonon up to $n=6$. The overtones of the Γ_5 phonon were obtained using the method of Ref. 14. It was necessary to consider overtones up to order $n=6$ for the Γ_3 phonon, and $n=10$ for the Γ_3 phonon, in order to obtain convergence in the energy values of the vibronic states.

Symmetry-adapted vibronic states, i.e., combinations of products of electronic and vibrational states, were obtained using the Clebsch-Gordan coefficients for the group T_d as found, for example, in Ref. 1. We do not display these states to save space. Here we mention a few examples. The state $|\alpha A(0)\rangle$ belonging to Γ_1 is a product of the electronic state $|\alpha\rangle$ and of the phonon vacuum state $A(0)=|0,0\rangle=|0,0,0\rangle$. The state

$$2^{-1/2}[|\gamma_1 C^{(3)}_1(1)\rangle+|\gamma_2 C^{(3)}_2(1)\rangle]$$

also belongs to Γ_1 as follows from Unsöld's theorem. The set

$$-\tfrac{1}{2}|\epsilon_1 C_1(n)\rangle+\tfrac{1}{2}\sqrt{3}|\epsilon_1 C_2(n)\rangle\ ,$$

$$-\tfrac{1}{2}|\epsilon_2 C_1(n)\rangle-\tfrac{1}{2}\sqrt{3}|\epsilon_2 C_2(n)\rangle\ ,$$

and

$$|\epsilon_3 C_1(n)\rangle$$

generates the Γ_5 representation of the group (for $n \geq 1$). Even though the Γ_5 phonons do not couple to the electronic ${}^5\Gamma_3$ states via H_{ep}, it is necessary to include in our basis the states involving electronic levels in the ${}^5\Gamma_3$ manifold and Γ_5 phonons. The reason for this is that the spin-orbit interaction alters the spacing of the levels after modification by H_{ep}. However, a good approximation is

TABLE III. Symmetrized overtones of a $\Gamma_3(T_d)$ phonon of order n ($0 \leq n \leq 6$).

n	Symmetry		State
0	Γ_1	$A^{(3)}(0)$	$\|0,0\rangle$
1	Γ_3	$C^{(3)}_1(1)$	$\|1,0\rangle$
		$C^{(3)}_2(1)$	$\|0,1\rangle$
2	Γ_1	$A^{(3)}(2)$	$\frac{1}{\sqrt{2}}\|2,0\rangle+\frac{1}{\sqrt{2}}\|0,2\rangle$
	Γ_3	$C^{(3)}_1(2)$	$\frac{1}{\sqrt{2}}\|2,0\rangle-\frac{1}{\sqrt{2}}\|0,2\rangle$
		$C^{(3)}_2(2)$	$-\|1,1\rangle$
3	Γ_1	$A^{(3)}(3)$	$\frac{1}{2}\|3,0\rangle-\frac{1}{2}\sqrt{3}\|1,2\rangle$
	Γ_2	$B^{(3)}(3)$	$\frac{1}{2}\|0,3\rangle-\frac{1}{2}\sqrt{3}\|2,1\rangle$
	Γ_3	$C^{(3)}_1(3)$	$\frac{1}{2}\sqrt{3}\|3,0\rangle+\frac{1}{2}\|1,2\rangle$
		$C^{(3)}_2(3)$	$\frac{1}{2}\sqrt{3}\|0,3\rangle+\frac{1}{2}\|2,1\rangle$
4	Γ_1	$A^{(3)}(4)$	$\sqrt{\frac{3}{8}}\|4,0\rangle+\sqrt{\frac{3}{8}}\|0,4\rangle+\frac{1}{2}\|2,2\rangle$
	Γ_3	$C^{(3)}_1(4)$	$\frac{1}{\sqrt{2}}\|4,0\rangle-\frac{1}{\sqrt{2}}\|0,4\rangle$
		$C^{(3)}_2(4)$	$-\frac{1}{\sqrt{2}}\|3,1\rangle-\frac{1}{\sqrt{2}}\|1,3\rangle$
	Γ_3	$C'^{(3)}_1(4)$	$\frac{1}{\sqrt{8}}\|4,0\rangle+\frac{1}{\sqrt{8}}\|0,4\rangle-\frac{1}{2}\sqrt{3}\|2,2\rangle$
		$C'^{(3)}_2(4)$	$\frac{1}{\sqrt{2}}\|3,1\rangle-\frac{1}{\sqrt{2}}\|1,3\rangle$
5	Γ_1	$A^{(3)}(5)$	$\frac{\sqrt{5}}{4}\|5,0\rangle-\frac{\sqrt{2}}{4}\|3,2\rangle-\frac{3}{4}\|1,4\rangle$
	Γ_2	$B^{(3)}(5)$	$-\frac{3}{4}\|4,1\rangle-\frac{\sqrt{2}}{4}\|2,3\rangle+\frac{\sqrt{5}}{4}\|0,5\rangle$
	Γ_3	$C^{(3)}_1(5)$	$\frac{3}{\sqrt{11}}\|3,2\rangle-\sqrt{\frac{2}{11}}\|1,4\rangle$
		$C^{(3)}_2(5)$	$\frac{3}{\sqrt{22}}\|4,1\rangle-\frac{2}{\sqrt{11}}\|2,3\rangle+\sqrt{\frac{5}{22}}\|0,5\rangle$
	Γ_3	$C'^{(3)}_1(5)$	$\frac{1}{4}\sqrt{\frac{10}{11}}\|3,2\rangle+\frac{3}{4}\sqrt{\frac{5}{11}}\|1,4\rangle+\sqrt{\frac{11}{4}}\|5,0\rangle$
		$C'^{(3)}_2(5)$	$\frac{3}{4}\sqrt{\frac{10}{11}}\|2,3\rangle+\frac{1}{4}\sqrt{\frac{5}{11}}\|4,1\rangle+\frac{9}{4\sqrt{11}}\|0,5\rangle$
6	Γ_1	$A^{(3)}(6)$	$\frac{1}{4}(\sqrt{5}\|6,0\rangle+\sqrt{5}\|0,6\rangle+\sqrt{3}\|4,2\rangle+\sqrt{3}\|2,4\rangle)$
	Γ_1	$A'^{(3)}(6)$	$\frac{1}{4\sqrt{2}}(\|6,0\rangle-\|0,6\rangle-\sqrt{15}\|4,2\rangle+\sqrt{15}\|2,4\rangle)$
	Γ_2	$B^{(3)}(6)$	$\frac{1}{4}(\sqrt{10}\|3,3\rangle-\sqrt{3}\|5,1\rangle-\sqrt{3}\|1,5\rangle)$
	Γ_3	$C^{(3)}_1(6)$	$\frac{1}{4\sqrt{2}}(\sqrt{15}\|6,0\rangle-\sqrt{15}\|0,6\rangle+\|4,2\rangle-\|2,4\rangle)$
		$C^{(3)}_2(6)$	$-\frac{1}{4}(\sqrt{5}\|5,1\rangle+\sqrt{5}\|1,5\rangle+\sqrt{6}\|3,3\rangle)$
	Γ_3	$C'^{(3)}_1(6)$	$\frac{1}{4}(\sqrt{3}\|6,0\rangle+\sqrt{6}\|0,6\rangle-\sqrt{5}\|4,2\rangle-\sqrt{5}\|2,4\rangle)$
		$C'^{(3)}_2(6)$	$\frac{1}{\sqrt{2}}(\|5,1\rangle-\|1,5\rangle)$

obtained by restricting the basis to states containing overtones of only one vibrational mode.

With the set of basis vectors obtained in this fashion, we can proceed with the diagonalization of the Hamiltonian matrix. The dimensions of the Γ_1, Γ_2, Γ_3, Γ_4, and Γ_5 matrices are 342, 321, 659, 965, and 983, respectively.

To make contact with the experimental data in CdTe:Fe^{2+} we must select the parameters $\hbar\omega_3$, $\hbar\omega_5$, $E_{JT}^{(3)}$, $E_{JT}^{(5)}$, Δ, λ, and ρ in a way consistent with the known characteristics of the host crystal and the magnetic ion. Several choices of these parameters were tried. The final results were obtained in the following way. We first fixed $\hbar\omega_3$ and $\hbar\omega_5$ to agree with those of Refs. 7 and 14, and selected values of λ and ρ near the known values for the free ion[16] (namely $\lambda=-104$ cm^{-1} and $\rho=1.04$ cm^{-1}). A tentative value of Δ was selected and λ, ρ, and $E_{JT}^{(3)}$ were varied to fit the transitions in the far infrared. These do not depend critically on the choice of Δ in the vicinity of 2500 cm^{-1}. The value of the $^5\Gamma_5-{}^5\Gamma_3$ orbital splitting Δ was adjusted using the transition labeled I by Udo *et al.*,[6] varying $E_{JT}^{(5)}$. The present value of Δ differs from that of Ref. 6 because of the downward shift of the lowest level in the $^5\Gamma_5$ multiplet due to the Jahn-Teller interaction. We note that the range of values of $E_{JT}^{(3)}$ and $E_{JT}^{(5)}$ yielding a satisfactory fit to the data is rather narrow. Figures 1 and 2 show the dependence of the lower-lying energy levels in the $^5\Gamma_3$ and $^5\Gamma_5$ multiplets as functions of $E_{JT}^{(3)}$ and $E_{JT}^{(5)}$, respectively. It is necessary to recognize that, via the spin-orbit interaction, the dynamic Jahn-Teller effect in the $^5\Gamma_5$ multiplet modifies the energy-level spacings in the $^5\Gamma_3$ multiplet. The choice of λ and ρ is not unique but is limited to a narrow range. Besides our preferred choice ($\lambda=-95$ cm^{-1} and $\rho=0.7$ cm^{-1}), satisfactory agreement was also obtained with $\lambda=-102$ cm^{-1} and $\rho=0.18$ cm^{-1}.

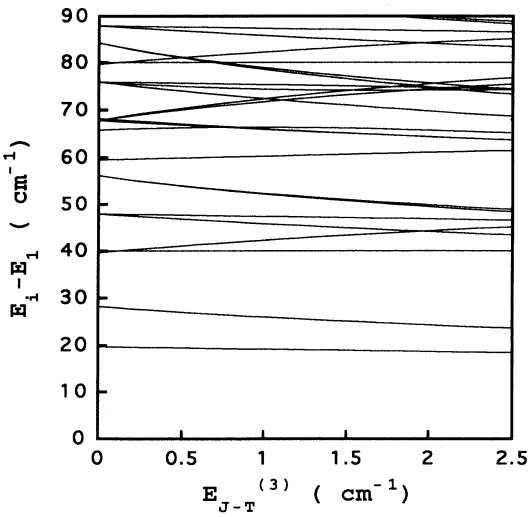

FIG. 1. Energy levels of the low-lying vibronic levels originating from the $^5\Gamma_3$ multiplet of Fe^{2+} in CdTe as functions of the Jahn-Teller energy $E_{JT}^{(3)}$ describing the interaction between the electronic $^5\Gamma_3$ states and the Γ_3 phonon. The remaining parameters are those specified in the text. The energies are measured from the ground state E_1.

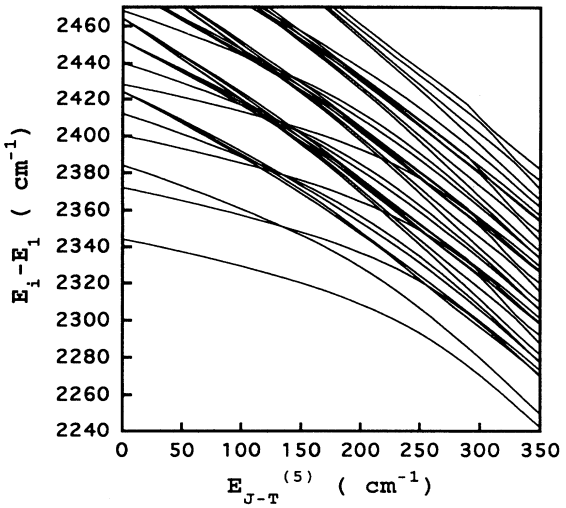

FIG. 2. Energy levels of the lower vibronic levels originating from the $^5\Gamma_5$ multiplet of Fe^{2+} in CdTe as functions of $E_{JT}^{(5)}$ measured from the ground state E_1. The remaining parameters are given in the text.

The energy levels of the system are labeled by the irreducible representation of T_d to which they belong. In Table IV we list those states which we attribute to the observed transitions, including the experimental and calculated values of the transition energies. We give their symmetry by the index 1,2,. . .,5 of the irreducible representation in the notation of Koster *et al.*[1] and an alphabetical index which simply gives the order of increasing energy. The first Γ_5 level, for example, is labeled by 5, the second (in the $^5\Gamma_5$ multiplet) by 5′, and the third by

TABLE IV. Energies and oscillator strengths of far- and near-infrared transitions in $Cd_{1-x}Fe_xTe$. The first column gives the theoretical assignments of the lines. Columns 3 and 4 give a comparison between experimental and calculated transition energies. In the last column are the calculated values of the oscillator strengths. The experimental labels are those of Ref. 6. Parameters used are $\Delta=2529.9$ cm^{-1}, $\lambda=-95$ cm^{-1}, $\rho=0.7$ cm^{-1}, $\hbar\omega_3=28$ cm^{-1}, $\hbar\omega_5=40$ cm^{-1}, $E_{JT}^{(3)}=1.97$ cm^{-1}, and $E_{JT}^{(5)}=275$ cm^{-1}.

Transition	Expt. label	Expt. energy (cm^{-1})	Calculated energy (cm^{-1})	Oscillator strength
$1\rightarrow 4$		18.6[a]	18.7	1.60×10^{-7}
$1\rightarrow 5c$		66.0[a]	65.7	4.14×10^{-7}
$1\rightarrow 5d$		74.0[a]	74.2	3.15×10^{-7}
$5b\rightarrow 5'a$	*IV*	2231.9[b]	2232.8	3.19×10^{-5}
$3\rightarrow 5'$	*III*	2256.3[b]	2258.5	1.69×10^{-5}
$4\rightarrow 5'$	*II*	2264.1[b]	2264.2	3.24×10^{-4}
$4\rightarrow 5'a$	X_{II}	2275.1[b]	2275.1	1.22×10^{-4}
$1\rightarrow 5'$	*I*	2282.8[b]	2282.9	1.23×10^{-4}
$1\rightarrow 5'a$	X_I	2293.8[b]	2293.9	1.04×10^{-4}
$1\rightarrow 5'b$	*Y*	2309.0[b]	2309.0	1.05×10^{-4}
$1\rightarrow 5'c$			2312.2	6.04×10^{-5}
$1\rightarrow 5'd$		2317.8[b]	2318.9	8.42×10^{-5}

[a]Reference 7.
[b]Reference 6.

5'', with obvious similar notations for the other states. $E_{JT}^{(5)}$ was adjusted so that the spacings between lines I, X_I, and Y agree with the near-infrared data[6] and $E_{JT}^{(3)}$ to yield agreement with the far-infrared data.[5,7] Figure 3 graphically shows the procedure followed. In the lower part of the figure all parameters are fixed at the values listed in Table IV except $E_{JT}^{(3)}$, while a similar situation prevails in the upper part except that $E_{JT}^{(5)}$ is allowed to vary. The dashed vertical line shows the adjustment of $E_{JT}^{(3)}$ and $E_{JT}^{(5)}$ to the spacings of the transitions which we attribute to the observed lines.

IV. SELECTION RULES AND OSCILLATOR STRENGTHS

Table V gives selection rules for electric-dipole (E) and magnetic-dipole (M) transitions between energy levels of a quantum system in a tetrahedral field.

Electric-dipole transitions between the levels originating from the $3d^6$ configuration in the free ion are, of course, forbidden because of their parity. However, the tetrahedral potential lacks inversion symmetry and,

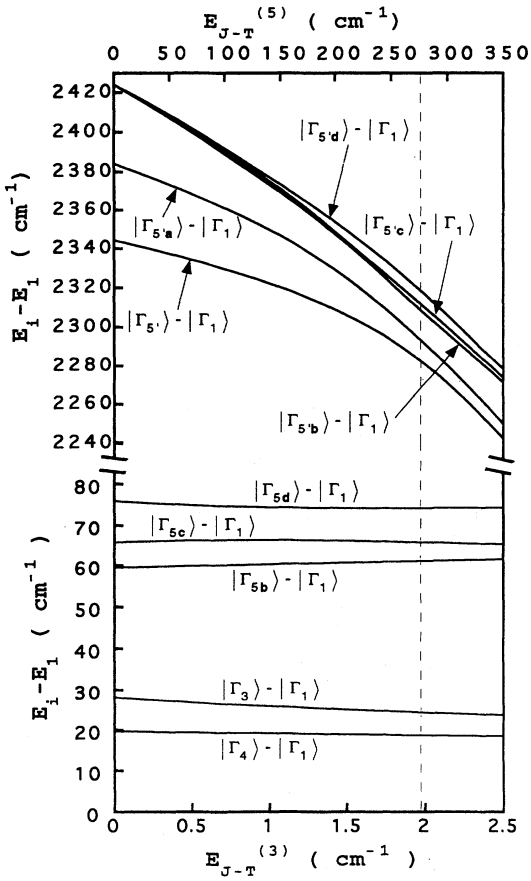

FIG. 3. The transitions attributed to the experimentally observed lines. In the upper part of the figure the calculated energies are given as functions of $E_{JT}^{(5)}$ with the remaining parameters as in the text. In the lower part of the figure the transition energies are displayed as functions of $E_{JT}^{(3)}$. The vertical dashed line represents the best fit to the far- and near-infrared absorption data (Refs. 2–7).

TABLE V. Selection rules for optical transitions: electric dipole (E), magnetic dipole (M), and forbidden (F) in the dipole (electric or magnetic) approximation.

	Γ_1	Γ_2	Γ_3	Γ_4	Γ_5
Γ_1	F	F	F	M	E
Γ_2	F	F	F	E	M
Γ_3	F	F	F	E,M	E,M
Γ_4	M	E	E,M	E,M	E,M
Γ_5	E	M	E,M	E,M	E,M

hence, mixes the $3d^6$ configuration with odd-parity states in the configurations $3d^5 4p$ and $3d^5 4f$. This mixing has been calculated by Savona, Bassani, and Rodriguez.[14] It is shown that the transition probability depends on a single matrix element denoted by $\langle \epsilon_3 | \sum_a z_a | \gamma_1 \rangle$, where states ϵ_3 and γ_1 are the orbital states defined in Sec. II corrected in first-order perturbation to include the admixture of odd-parity states resulting from that part of the tetrahedral potential which behaves as xyz. The sum over a includes all electrons in the ion. Within the point-ion approximation the coefficient associated with this term in the T_d potential equals $(20/\sqrt{3})ze^2R^{-4}$, where z is the effective charge (taken here equal to 2) and R is the nearest-neighbor distance. For CdTe, $R=2.8$ Å. This model yields a value of the spacing Δ seven times smaller than that observed.[14] Thus we conclude that the crystal is not purely ionic but is also significantly covalent. Instead of the nearest-neighbor distance one should substitute the distance from the magnetic ion site to the center of charge of the ligands. From the experimental value of Δ we estimate this distance to be $R \approx 2$ Å. Using the results of Ref. 14, we find

$$\left\langle \epsilon_3 \left| \sum_a z_a \right| \gamma_1 \right\rangle = 0.07 \text{ Å} ,$$

in good agreement with the value obtained in Ref. 7 from the ratio of electric-dipole to magnetic-dipole intensities.

The oscillator strength for an electric-dipole transition between states i and j of degeneracies l_i and l_j, respectively, is

$$f_E(i,j) = (2m\omega_{ij}/\hbar)[(\epsilon_\infty + 2)/3]^2 \times \sum_{\kappa_i=1}^{l_i} \sum_{\kappa_j=1}^{l_j} \left| \langle \Gamma_j, \kappa_j | \sum_a \mathbf{r}_a \cdot \hat{\epsilon} | \Gamma_i, \kappa_i \rangle \right|^2 . \quad (6)$$

Here $\hbar\omega_{ij}$ is the energy separation between states i and j, ϵ_∞ (for CdTe, $\epsilon_\infty = 7.1$), the optical dielectric constant of the crystal, $\hat{\epsilon}$, the polarization of the incident radiation, m, the free-electron mass, and the states are labeled by their irreducible representations and the rows κ_i and κ_j to which they belong.

The oscillator strength for the magnetic transitions is given by

$$f_M(i,j) = (\hbar\omega_{ij}\epsilon_\infty/2mc^2) \times \sum_{\kappa=1}^{l_i} \sum_{\kappa_j=1}^{l_j} |\langle \Gamma_j, \kappa_j | (\mathbf{L}+2\mathbf{S}) \cdot (\hat{\epsilon} \times \hat{k}) | \Gamma_i, \kappa_i \rangle|^2 \quad (7)$$

where $\hat{k}$ is the unit vector parallel to the direction of propagation of the incident radiation.

We have calculated the oscillator strengths for the transitions which we attribute to those observed. These are listed in the last column on the right-hand side of Table IV. The $\Gamma_1 \rightarrow \Gamma_4$ transition is purely magnetic dipole allowed. The $\Gamma_1 \rightarrow \Gamma_5$ is only electric dipole allowed while the oscillator strength of the $\Gamma_4 \rightarrow \Gamma_5$ transitions contains contributions from both electric-dipole and magnetic-dipole matrix elements. In this calculation use is made of wave functions obtained numerically in the diagonalization of the effective Hamiltonian described in Sec. III. The most important terms in these wave functions are given in Table VI. For ease of reading we have deleted the superscripts 3 and 5 in the labeling of the phonon overtones. The following must be noted: (i) For levels $|1\rangle$, $|3\rangle$, $|5c\rangle$, and $|5d\rangle$ all phonon overtones have symmetry Γ_3; (ii) $|4\rangle$ and $|5b\rangle$ contain phonon overtones of symmetry Γ_5 (labeled E), while the remaining overtones have symmetry Γ_3; (iii) all other levels listed show only Γ_5-phonon overtones; (iv) $A(0)$ is the phonon vacuum; and (v) the wave functions in Table VI contain additional terms involving phonons of either symmetry with coefficients which are too small to be significant and that are, therefore, not listed.

As an example we mention that the oscillator strength of the $\Gamma_4 \rightarrow \Gamma_{5d}$ line is obtained adding the contributions of electric-dipole and magnetic-dipole transitions in quadrature. The electric-dipole oscillator strength is 9.11×10^{-8}, while the magnetic-dipole oscillator strength is 4.29×10^{-8}. Of course, this transition is very weak at low temperatures because then the population of the Γ_4 level is small.

When they are allowed, electric-dipole and magnetic-dipole transitions are often comparable between states in the ${}^5\Gamma_3$ multiplet. The reasons for this is that the electric-dipole transitions are induced by the mixing of negative-parity states and additional mixing of ${}^5\Gamma_3$ and ${}^5\Gamma_5$ levels by the spin-orbit interaction. The magnetic-dipole transitions, on the other hand, do not require mixing with odd-parity states.

V. DISCUSSION

The observed transitions between levels in the ${}^5\Gamma_3$ multiplet are of two types. We attribute three of them, occurring at 18.6, 66, and 74 cm^{-1}, as originating from the lowest level, namely Γ_1. The final state of the line labeled $1 \rightarrow 4$ in Table IV is essentially a purely electronic state with small phonon and higher multiplet mixing. The final state of the line $1 \rightarrow 5c$ is again an electronic Γ_5 level with a substantial component containing a Γ_3 phonon. The most important contributions to the matrix element of the electric-dipole moment are

$$\langle \epsilon_3 A(0) | \sum_a z_a | \alpha' A(0) \rangle ,$$

$$\langle \epsilon_3' A(0) | \sum_a z_a | \alpha A(0) \rangle ,$$

and

$$\langle \epsilon_3'' A(0) | \sum_a z_a | \alpha A(0) \rangle .$$

In contrast, in $1 \rightarrow 5d$, $|5d\rangle$ has a large contribution of the state $|\delta_3 C_2(2)\rangle$, but the transition is dominated by matrix elements of the electric-dipole moment between the zero-phonon components in $|5d\rangle$ and $|\alpha A(0)\rangle$ in $|1\rangle$.

A transition labeled $4 \rightarrow 5d$ at 55.4 cm^{-1} has a significant oscillator strength of 1.24×10^{-7}. However, it should not be observed at low temperatures. A line at 54 cm^{-1} is observed by Lu *et al.*[17] in $Cd_{0.99}Fe_{0.01}Te$ which is absent in the spectrum of CdTe. The temperature dependence of its intensity is consistent with that of a local vibrational mode. To the right of this line, Lu *et al.* display a shoulder at 57 cm^{-1} which is not observed in Ref. 7 except for a slight asymmetry. Thus we may attribute this feature to the $4 \rightarrow 5d$ transition.

The parameters have been adjusted so that the calculated positions of lines I and X_I agree with experiment.[2,6] Line Y is attributed to an electric-dipole transition from the ground state $|1\rangle$ to $|5'b\rangle$, the third vibronic state associated with the lowest Γ_5 level in the ${}^5\Gamma_5$ multiplet which has only small phonon admixture. The line labelled $1 \rightarrow 5'd$ is correlated with the shoulder on the right of line Y, and is obtained in our calculation without further adjustment of parameters. This should has been observed experimentally in Refs. 2 and 6 as well as by Vogel *et al.*,[18] who carried out absorption as well as luminescence measurements in $CdTe:Fe^{2+}$. Their absorption spectrum reproduces the features observed by Udo *et al.*[6] Their lines $L1$ and $L2$ correspond to I and II, in the notation of Ref. 6 and the features at 2293 and 2309 cm^{-1} correspond to X_I and Y. The additional structure associated with the $1 \rightarrow 5'c$ transition at 2312 cm^{-1} is not reported in the existing experimental results.

The position, intensity, and temperature dependence of the line associated with the $4 \rightarrow 5'$ transition are in excellent correspondence with the observed results for the line labeled II in Ref. 6. The calculated ratio of the intensities of lines I and II at 4.5 K is 1.5×10^2, which compares favorably with the experimental value 1.1×10^2 reported by Udo *et al.*[6]

The calculated intensities of the lines $1 \rightarrow 5'a$ and $1 \rightarrow 5'b$ identified with X_I and Y in Ref. 6 are comparable to each other and to that of line I. This agrees with the experimental results[6] for Fe concentration $\gtrsim 5 \times 10^{17}$ cm^{-3} in CdTe. However, at low iron concentration the measured intensity of line X_I is considerably smaller than that of line I (see Fig. 5 in Ref. 6). A possible interpretation of this result, advanced in Ref. 6, is that lines X_I and Y originate from antiferromagnetically coupled pairs of Fe^{2+} ions. At this time, we cannot give a quantitative analysis of this mechanism. Within the framework used in this paper we are not able to account for the decrease in the relative intensities of lines X_I and Y in relation to that of line I as the iron concentration decreases below 5×10^{17} cm^{-3}.

We identify the $3 \rightarrow 5'$ transition as the experimental line *III*. We note that the wave function of state $|3\rangle$ contains almost 90% of $|\alpha C_1(1)\rangle$, i.e., it is essentially the electronic ground state plus one Γ_e phonon of energy

$\hbar\omega_3$. This determines the energy of the initial state, namely 24.4 cm^{-1} above the ground state. However, the transition probability is determined essentially by the matrix element of the electric-dipole moment between $|\gamma_1 A(0)\rangle$ and $|\epsilon_3' A(0)\rangle$. Thus our interpretation differs from that in Ref. 6, where no phonon coupling was included.

We remark that the wave functions listed in Table VI

TABLE VI. Vibronic wave functions for the states involved in the transitions considered in Table IV.

Notation	E (cm^{-1})	Wave function
$\|1\rangle$	0	$0.9748\|\alpha A(0)\rangle - 0.1610\|\alpha' A(0)\rangle - 0.1491\left[\frac{1}{\sqrt{2}}\|\gamma_1 C_1(1)\rangle + \frac{1}{\sqrt{2}}\|\gamma_2 C_2(1)\rangle\right]$ $+0.0195\left[\frac{1}{\sqrt{2}}\|\gamma_1' C_1(1) + \frac{1}{\sqrt{2}}\|\gamma_2' C_2(1)\rangle\right] + 0.0272\|\alpha A(2)\rangle + \cdots$
$\|4\rangle$	18.7	$0.9525\|\delta_3 A(0)\rangle + 0.0900\|\delta_3' A(0)\rangle - 0.1119\|\delta_3'' A(0)\rangle - 0.2421\|\delta_3 C_1(1)\rangle$ $+0.0316\left[\frac{1}{\sqrt{2}}\|\delta_1 E_2(1)\rangle + \frac{1}{\sqrt{2}}\|\delta_2 E_1(1)\rangle\right] - 0.0226\|\delta_3' C_1(1)\rangle + 0.0281\|\delta_3'' C_1(1)\rangle$ $-0.0927\|\epsilon_3 C_2(1)\rangle - 0.0191\|\delta_3 C_1(2)\rangle + 0.0430\|\delta_3 A(2)\rangle + \cdots$
$\|3\rangle$	24.4	$-0.3876\|\gamma_1 A(0)\rangle + 0.0518\|\gamma_1' A(0)\rangle + 0.8935\|\alpha C_1(1)\rangle - 0.1469\|\alpha' C_1(1)\rangle + \cdots$
$\|5b\rangle$	61.0	$0.0638\|\epsilon_3 A(0)\rangle + 0.9848\left[\frac{1}{\sqrt{2}}\|\delta_1 E_2(1)\rangle - \frac{1}{\sqrt{2}}\|\delta_2 E_1(1)\rangle\right] + 0.0106\|\epsilon_3' A(0)\rangle$ $+0.0934\left[\frac{1}{\sqrt{2}}\|\delta_1' E_2(1)\rangle - \frac{1}{\sqrt{2}}\|\delta_2' E_1(1)\rangle\right] - 0.1163\left[\frac{1}{\sqrt{2}}\|\delta_1'' E_2(1)\rangle - \frac{1}{\sqrt{2}}\|\delta_2''\ E_1(1)\rangle\right] + \cdots$
$\|5c\rangle$	65.7	$0.8016\|\epsilon_3 A(0)\rangle + 0.0652\|\epsilon_3' A(0)\rangle + 0.0429\|\epsilon_3'' A(0)\rangle + 0.1488\|\delta_3 C_2(1)\rangle$ $+0.3239\|\epsilon_3 C_1(1)\rangle + 0.4369\|\delta_3 C_2(2)\rangle - 0.0510\|\delta_3'' C_2(2)\rangle + 0.0483\|\epsilon_3 C_1(2)\rangle + \cdots$
$\|5d\rangle$	74.2	$-0.4397\|\epsilon_3 A(0)\rangle - 0.0361\|\epsilon_3' A(0)\rangle - 0.0236\|\epsilon_3'' A(0)\rangle - 0.3131\|\delta_3 C_2(1)\rangle$ $+0.0992\|\epsilon_3 C_1(1)\rangle + 0.7546\|\delta_3 C_2(2)\rangle - 0.2627\|\delta_3 B(3)\rangle + \cdots$
$\|5'\rangle$	2282.9	$0.4598\|\epsilon_3' A(0)\rangle - 0.0406\|\epsilon_3 A(0)\rangle + 0.0269\|\epsilon_3'' A(0)\rangle + 0.4064\|\epsilon_3' A(2)\rangle$ $-0.3179\left[\frac{1}{\sqrt{2}}\|\epsilon_1' E_2(1)\rangle + \frac{1}{\sqrt{2}}\|\epsilon_2' E_1(1)\rangle\right] - 0.0972\left[\frac{1}{\sqrt{2}}\|\epsilon_1'' E_2(1)\rangle + \frac{1}{\sqrt{2}}\|\epsilon_2''\ E_1(1)\rangle\right]$
$\|5'a\rangle$	2293.9	$-0.0255\|\epsilon_3 A(0)\rangle + 0.3420\|\epsilon_3' A(0)\rangle - 0.0486\|\epsilon_3'' A(0)\rangle$ $+0.1124\|\gamma_1' E_3(1)\rangle - 0.1181\left[\frac{1}{\sqrt{2}}\|\delta_1'' E_2(1)\rangle - \frac{1}{\sqrt{2}}\|\delta_2'' E_1(1)\rangle\right]$ $+0.2385\left[\frac{1}{\sqrt{2}}\|\epsilon_1' E_2(1)\rangle + \frac{1}{\sqrt{2}}\|\epsilon_2' E_1(1)\rangle\right]$ $+0.0172\|\gamma_1 E_3(1)\rangle - 0.0274\left[\frac{1}{\sqrt{2}}\|\delta_1 E_2(1)\rangle - \frac{1}{\sqrt{2}}\|\delta_2 E_1(1)\rangle\right]$ $+0.0894\left[\frac{1}{\sqrt{2}}\|\delta_1' E_2(1)\rangle - \frac{1}{\sqrt{2}}\|\delta_2' E_1(1)\rangle\right]$ $-0.0170\left[\frac{1}{\sqrt{2}}\|\epsilon_1 E_2(1)\rangle + \frac{1}{\sqrt{2}}\|\epsilon_2 E_1(1)\rangle\right]$ $-0.0499\left[\frac{1}{\sqrt{2}}\|\epsilon_1'' E_2(1)\rangle + \frac{1}{\sqrt{2}}\|\epsilon_2'' E_1(1)\rangle\right] + \cdots$
$\|5'b\rangle$	2309.0	$0.4263\|\epsilon_3' A(0)\rangle + 0.0280\|\epsilon_3'' A(0)\rangle - 0.0374\|\epsilon_3 A(0)\rangle$ $-0.3404\left[\frac{1}{\sqrt{2}}\|\epsilon_1' E_2(1)\rangle + \frac{1}{\sqrt{2}}\|\epsilon_2' E_1(1)\rangle\right] + \cdots$
$\|5'c\rangle$	2312.2	$0.0251\|\epsilon_3 A(0)\rangle - 0.3049\|\epsilon_3' A(0)\rangle + 0.4475\|\epsilon_3' C_1(2)\rangle + 0.3376\|\epsilon_3' C_1(4)\rangle + \cdots$
$\|5'd\rangle$	2318.9	$0.0197\|\epsilon_3 A(0)\rangle - 0.2863\|\epsilon_3' A(0)\rangle + 0.069\|\epsilon_3'' A(0)\rangle$ $-0.2888\left[\frac{1}{\sqrt{2}}\|\epsilon_1' E_2(1)\rangle + \frac{1}{\sqrt{2}}\|\epsilon_2' E_1(1)\rangle\right] + \cdots$

are not complete, as indicated by appropriate ellipses. We have listed the most important terms but additional components were not displayed. These will appear in the doctoral thesis of one of the authors (D.C.).

ACKNOWLEDGMENTS

The authors wish to thank Professor A. K. Ramdas for many useful discussions. This work was supported by the U.S. National Science Foundation (Materials Research Group Grant No. DMR 92-21390), by the North Atlantic Treaty Organization (Research Grant No. 890866), by the Fonds National de la Recherche Scientifique (Belgium), by Academic Research Collaboration between Fonds National de la Recherche Scientifique, the Commissariat Général aux Relations Internationales and the British Council, 1994-95 (BEL-03666-2) and by the Nuffield Foundation (M.V.; Grant No. SCI-180-92-289-G). One of the authors (E.K.) wishes to acknowledge the hospitality of Professor Arnold Tubis and his colleagues during his stay at Purdue University when this work was completed.

APPENDIX

The matrix elements of $\mathbf{L}\cdot\mathbf{S}$ between states of the same symmetry in the wave functions listed in Tables I and II are

$$\begin{bmatrix} 0 & -2\sqrt{6} \\ -2\sqrt{6} & -2 \end{bmatrix} \tag{A1}$$

for the $|\alpha\rangle, |\alpha'\rangle$ submatrix;

$$\begin{bmatrix} 0 & -2\sqrt{3} \\ -2\sqrt{3} & 1 \end{bmatrix} \tag{A2}$$

for the pair $|\gamma_i\rangle, |\gamma_i'\rangle$ ($i=1$ and 2);

$$\begin{bmatrix} 0 & \sqrt{6} & -2\sqrt{3} \\ \sqrt{6} & 1 & 0 \\ -2\sqrt{3} & 0 & -2 \end{bmatrix} \tag{A3}$$

for ($|\delta_i\rangle, |\delta_i'\rangle, |\delta_i''\rangle$), ($i=1$, 2, and 3); and

$$\begin{bmatrix} 0 & 3(\frac{2}{5})^{1/2} & 2(\frac{3}{5})^{1/2} \\ 3(\frac{2}{5})^{1/2} & 3 & 0 \\ 2(\frac{3}{5})^{1/2} & 0 & -2 \end{bmatrix} \tag{A4}$$

for the three states $|\epsilon_i\rangle$, $|\epsilon_i'\rangle$, and $|\epsilon_i''\rangle$ ($i=1$, 2, and 3).

[1] G. F. Koster, J. O. Dimmock, R. G. Wheeler, and H. Statz, *Properties of the Thirty-two Point Groups* (MIT, Cambridge, MA, 1966).

[2] G. A. Slack, F. S. Ham, and R. M. Chrenko, Phys. Rev. **152**, 376 (1966). This paper contains references to early work on transition-metal ions in tetrahedral environments.

[3] J. M. Baranowski, J. W. Allen, and G. L. Pearson, Phys. Rev. **160**, 627 (1967).

[4] G. A. Slack, S. Roberts, and F. S. Ham, Phys. Rev. **155**, 170 (1967).

[5] G. A. Slack, S. Roberts, and J. T. Vallin, Phys. Rev. **187**, 511 (1969).

[6] M. K. Udo, M. Villeret, I. Miotkowski, A. J. Mayur, A. K. Ramdas, and S. Rodriguez, Phys. Rev. B **46**, 7459 (1992).

[7] C. Testelin, C. Rigaux, A. Mauger, A. Mycielski, and C. Julien, Phys. Rev. B **46**, 2183 (1992).

[8] H. A. Jahn and E. Teller, Proc. R. Soc. London Ser. A **161**, 220 (1937).

[9] Reviews of the Jahn-Teller effect as applied to solids have been given by M. D. Sturge, in *Solid State Physics,* edited by F. Seitz, D. Turnbull, and H. Ehrenreich (Academic, New York, 1967), Vol. 20, p. 91, and by F. S. Ham, in *Electron Paramagnetic Resonance,* edited by S. Geschwind (Plenum, New York, 1970). See also F. S. Ham, Phys. Rev. **138**, A1727 (1965); **166**, 307 (1968). Additional details and references can be found in I. B. Bersuker and V. Z. Polinger, *Vibronic Interactions in Molecules and Crystals* (Springer, Berlin, 1989).

[10] J. T. Vallin, Phys. Rev. B **2**, 2390 (1970).

[11] J. Rivera-Iratchet, M. A. de Orúe, and E. E. Vogel, Phys. Rev. B **34**, 3992 (1986). See also J. Rivera-Iratchet, M. A. de Orúe, M. L. Flores, and E. E. Vogel, *ibid.* **47**, 10 164 (1993); E. E. Vogel and J. Rivera-Iratchet, *ibid.* **22**, 4511 (1980).

[12] L. Martinelli, M. Passaro, and G. Pastori Parravicini, Phys. Rev. B **39**, 13 343 (1989).

[13] R. Haydock, in *Solid State Physics,* edited by H. Ehrenreich, F. Seitz, and D. Turnbull (London, Academic, 1980), Vol. 35, pp. 215–294.

[14] V. Savona, F. Bassani, and S. Rodriguez, Phys. Rev. B **49**, 2408 (1994).

[15] See, for example, A. Abragam and B. Bleaney, *Electron Paramagnetic Resonance of Transition Ions* (Clarendon, Oxford, 1970), p. 398.

[16] These parameters are quoted in F. S. Ham and G. A. Slack, Phys. Rev. B **4**, 777 (1971) based on a least-squares fit to the spectroscopic data in C. E. Moore, *Atomic Energy Levels,* Natl. Bur. Stand. (U.S.) Circ. No. 467 (U.S. GPO, Washington, D.C., 1952), Vol. 2, p. 60.

[17] W. Lu, H. J. Ye, Z. Y. Yu, S. Y. Zhang, Y. Fu, W. L. Xu, S. C. Shen, and W. Giriat, Phys. Status Solidi B **147**, 767 (1988).

[18] E. E. Vogel, O. Mualin, M. A. de Orúe, J. Rivera-Iratchet, M. L. Flores, U. W. Pohl, H.-J. Schulz, and M. Thiede, Phys. Rev. B **50**, 5231 (1994) (see Fig. 2 in this reference).